High-fidelity anatomical phantoms for MRI practical training

Habeeb Yusuff, Pierre-Emmanuel Zorn, Franck Blindauer, Naji Kharouf, David Sémeril, Guillaume Bierry, Stéphane Kremer, Jean-Philippe Dillenseger

Physica Medica 127 (2024) 104832

Contents lists available at ScienceDirect

Physica Medica

journal homepage: www.elsevier.com/locate/ejmp

Technical Note

High-fidelity anatomical phantoms for MRI practical training

Y. Habeeb [a], P.E. Zorn [b], F. Blindauer [c], N. Kharouf [d,e], D. Semeril [f], G. Bierry [a,b,g], S. Kremer [a,b,g], J.P. Dillenseger [a,b,g,*]

[a] University of Strasbourg, CNRS, Inserm, ICube UMR 7357, Strasbourg, France
[b] Pôle d'imagerie médicale, Hôpitaux Universitaires de Strasbourg, Strasbourg, France
[c] Groupe d'imagerie médicale MIM, Strasbourg, France
[d] Department of Biomaterials and Bioengineering, INSERM UMR_S 1121, 67000 Strasbourg, France
[e] Faculty of Dental Medicine University of Strasbourg, 67000 Strasbourg, France
[f] UMR-CNRS 7177, Institut de Chimie de Strasbourg, Strasbourg, France
[g] Faculté de Médecine, Maïeutique et Sciences de la Santé, Université de Strasbourg, Strasbourg, France

ARTICLE INFO

Keywords:
Magnetic resonance imaging
Phantoms
Anatomy
3D printing

ABSTRACT

Introduction: Practical MRI training is essential for bridging the gap between complex theoretical knowledge and clinical applications. Traditional phantoms used in MRI, such as ACR phantoms, are valuable for illustrating system characterization methods but often lack the anatomical complexity required for realistic training. This study presents the development of high-fidelity anatomical phantoms designed specifically for practical MRI training. These phantoms replicate key anatomical structures and tissue contrasts of the head, offering a more realistic training experience for healthcare students and medical imaging staff (radiologists, physicists, radiographers).

Materials and Methods: We focused on the head region, creating phantoms from reference MRI T1-weighted slices and using computer-aided design (CAD) software to design detailed anatomical structures. These phantoms were 3D printed and filled with tissue-mimicking gels. MRI acquisitions were performed using a 1.5T clinical MRI system.

Results: The resulting images demonstrated high anatomical fidelity and realistic MRI tissue contrasts. The phantoms allow for effective demonstration of the impact of parameter modifications on MRI images and aid in anatomical structure recognition.

Conclusion: While technical improvements are needed to ensure long-term stability and accurate relaxometric properties, these phantoms hold significant potential for enhancing MRI education and sequences evaluations. The approach can be extended to other anatomical regions, further supporting the training and optimization of MRI sequences.

1. Introduction

Practical MRI training is essential for bridging the gap between complex theoretical concepts and clinical applications. Some health science faculties provide opportunities for practical MRI training, typically conducted in radiology units of university hospitals or research laboratories during dedicated and rare time slots. These on-site practical sessions generally employ quality assurance phantoms, such as ACR Phantoms [1–3], to illustrate MR system characterization methods (e.g., homogeneity, distortion) and the effects of parameters adjustments, sequences, or coils on image quality. Most MRI phantoms are constructed with separate compartments containing aqueous solutions of paramagnetic ions, designed to mimic tissue parameters such as T1, T2, Rho, and diffusion coefficients. Despite their utility, these phantoms, typically made with spheres and cylinders, lack the complexity of real anatomical structures.

For healthcare students and medical imaging staff (radiologists, radiographers), the use of such phantoms can seem too disconnected from the clinical reality that emphasizes morphological imaging and MRI tissue contrasts [4]. While performance evaluations regarding homogeneity, distortion, and other parameters are crucial from an engineering and research perspective, they do not align with the primary

* Corresponding author at: Faculté de Médecine, Maïeutique et Sciences de la Santé, 4, rue Kirschleger, 67000 Strasbourg, France.
E-mail address: jp.dillenseger@unistra.fr (J.P. Dillenseger).

https://doi.org/10.1016/j.ejmp.2024.104832
Received 25 July 2024; Received in revised form 14 September 2024; Accepted 28 September 2024
Available online 19 October 2024

educational needs of healthcare students. These students primarily aim to recognize anatomical structures and understand the impact of basic parameter changes on MRI contrast and image quality.

Consequently, during practical sessions, it is common for volunteer students to undergo MRI scanning while others, supervised by an instructor, adjust sequence parameters and generate images. Although this practice may be allowed under specific administrative frameworks, it remains ethically contentious [5]. To avoid complex administrative procedures and ethical dilemmas, a potential solution is the use of high-fidelity anatomical phantoms for training purposes. However, such phantoms are not well known, with only a few recent publications mentioning morphological phantoms [6–10] but they are lacking in high-fidelity anatomy on a user point of view.

This study presents the initial results of developing high-fidelity anatomical phantoms designed for practical MRI training.

2. Materials and methods

2.1. Morphological phantom design

In this study, we focused on the head anatomical region, frequently explored in MRI. Initially, we selected reference MRI slices to present the essential anatomical structures in this region:

- A sagittal median MRI slice
- A coronal MRI slice through the trunk
- A transverse MRI slice in through the anterior and posterior commissures

We manually drew the main anatomical structures of interest from these reference MRI slices (Fig. 1a) using Keynote software (Keynote v12.2.1, Apple Inc, Cupertino, USA) and created anatomical images (Fig. 1b) exported in.tiff format. These images served as the basis for CAD work using PTC-Creo (v10.0, Parametric Technology Corporation, Boston, USA). Each reference slice was integrated into a circular module with a diameter of 214 mm, with 20 mm high walls representing the boundaries (wall thickness: 0.5 mm) of the identified anatomical structures (Fig. 1c). All CAD files were exported in Stereo-lithography (STL) format, 3D printed (see 2.2), and filled with tissue-mimicking materials (TMM) (see 2.3) (Fig. 1d). The different steps of this phantom building process are shown in Fig. 1.

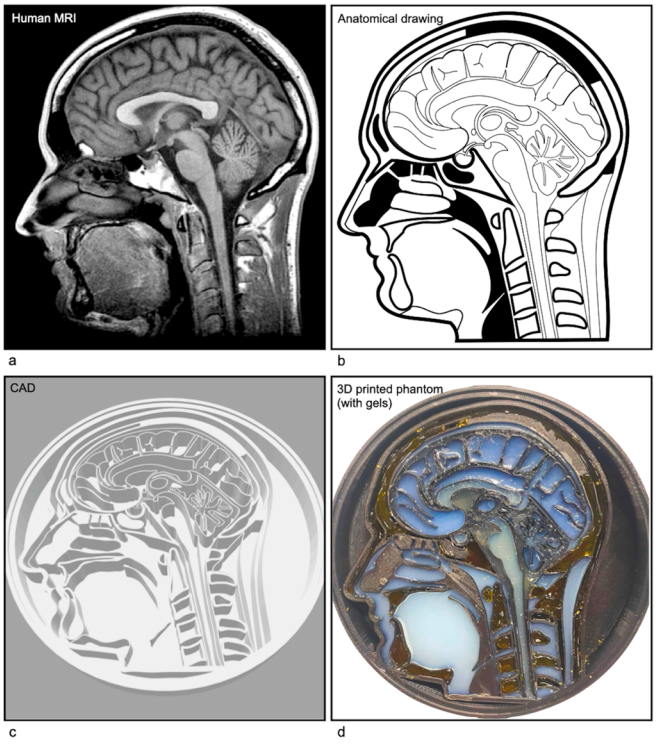

Fig. 1. Sagittal $T1_w$ human head MRI (a), anatomical drawing (b), CAD (c), 3D printed phantom filled with gels (d).

2.2. Printing methods

STL models were printed using PETG 1.75 mm filaments on a fused deposition modeling (FDM) printer (X1-Carbon, Bambu Lab, Shenzhen, China) with polyethylene-terephthalate-glycol (PETG) filament (Prusa Polymers, Prague, Czech Republic). G-code files for controlling the FDM 3D printer were generated using BambuStudio slicer (v1.9.1.67, Bambu Lab, Shenzhen, China), with printing parameters outlined in Table 1.

2.3. Tissue-mimicking materials (TMM) and phantom filling

We reviewed literature on TMM gels and selected specific articles [11–17] to guide our choices. We identifies that TMMs are generally composed of 4 elements: a gelling agent, one T1 modifier and one T2 modifier, and a preservative agent. Table 2 shows the chosen TMM gels and their compositions for tissues such as gray matter, white matter, muscle, and CSF [16,17]. We chose Carrageenan as a gelling agent coupled with gadolinium chloride ($GdCl_3$) as a T1 modifier and Agarose as a T2 modifier. We chose these materials because they didn't present any particular risks during the manufacturing process, and didn't impose any environmental restrictions.

Sodium azide (NaN_3) was added as preservative (antibacterial) agent. NaN_3 could be toxic, burns in air and may explode if large quantities are involved. Given the low proportions used (0.03 %), our quantities were very small. However, when we added this agent to our preparations, we decided to work in a fume hood.

For fat-containing structures (e.g., subcutaneous fat, bone marrow), we sought chemical shift properties enabling spectral saturation sequences, opting for soft polyvinyl chloride gels in a liquid plasticizer gel (PVCP or plastisol) [18]. The polyvinyl chloride must be mixed with the plasticizer at high temperature ($160 < T°C < 200°$), so precautions must be taken when handling.

To ensure longevity (limit the risk of gels dehydration), we sealed the top layer of the phantom with a thermoplastic film (Parafilm M, Bemis Company, Inc, Neenah, Wisconsin, USA).

2.4. MRI acquisitions

Experiments were conducted using a 1.5 T clinical MRI system (Ingenia Evolution, Philips Healthcare, Amsterdam, Netherlands) with a head receive coil (dStream 15 channels head coil, Philips Healthcare, Amsterdam, Netherlands). Phantoms were positioned in the center of the coil and imaged through four contrasts ($T1_w$, $T1_w$Spair, Rho_w and $T2_w$). Sequences parameters were detailed in Table 3.

3. Results

Figs. 2-5 present the MRI acquisition results. Fig. 2 displays the

Table 1
FDM 3D printing parameters.

FDM Printer model	X1-Carbon (Bambu Lab)
Nozzle	0.4 mm
Material/nozzle temperature/bed temperature	PETG/250 °C/60 °C
Infill/infill pattern	50 %/Grid
Layer height	0.2 mm
Print; Travel speed	50 to300 mm/s; 500 mm/s
printing duration (sag., cor., tra. phantoms)	9h28min, 7h53min, 11h17min

Table 2
Tissue mimiking materials compositions.

Tissue	Compositions			References
White matter	Carrageenan 3 % (gelling agent)	$GdCl_3$: 77.6 µmol/kg(T1 modifier)	Agarose: 0.439 % (T2 modifier)	[17] Min-Joo Kim et al
Grey matter	+ NaN3 0,03 % (preservative agent	$GdCl_3$ 14.7 µmol/kg (T1 modifier)	Agarose % 0.478 w/w (T2 modifier)	
Muscle		$GdCl_3$ 29.1 µmol/kg (T1 modifier)	Agarose 2.076 % w/w (T2 modifier)	
Cerebrospinal fluid		$GdCl_3$ 5.8 µmol/kg (T1 modifier)	/	/
Fat	PVC colloidal suspension 70 % Liquid ester plasticizer 30 %			[19] Chatelin et al.

Table 3
Sequences parameters.

	Acq.1	Acq.2	Acq.3	Acq.4
Sequence	Spin echo 2D	Spin echo 2D	Fast Spin echo 2D (dual echo)	Spin echo 2D
Contrast	$T1_w$	$T1_w$ – SPAIR	Rho_w; $T2_w$	T1w
FA	90°	90°	90°	90°
TR	500 ms	500 ms	41360 ms	500 ms/
TE	7,52 ms	7,52 ms	12,5ms-100 ms	9,8ms
Acq. Matrix (frequency × phase)	256 × 227	256 × 227	256 × 251	460 × 413
FOV	230 × 230 mm^2	230 × 230 mm^2	230 × 230 mm^2	230 × 230 mm^2
Acquired pixel size (frequency × phase)	0.89 × 1,01 mm^2	0.89 × 1,01 mm^2	0.89 × 0,91 mm^2	0.50 × 0,55 mm^2
Slice thickness	4 mm	4 mm	4 mm	4 mm
Pixel bandwidth	262 Hz	262 Hz	147 Hz	162 Hz
Sequence duration	355 s	539 s	177 s	417 s

contrasts obtained with these phantoms in different weightings, and Fig. 3 compares our phantoms contrasts ($T1_w$ and $T2_w$) with human acquisitions. Fig. 4 illustrates the phantoms' potential to highlight changes in geometric parameters (e.g., pixel size dimensions); and Fig. 5 shows the recognizable anatomical structures on the sagittal phantom.

We observed that, the relative intensities ranking of WM, GM and CSF in were respected the $T1_w$ and $T2_w$ contrasts (see Figs. 2 and 3). In T1w acquisition, The fat-TMM (PVCP) signal was higher than the muscle one which correspond to the expected tissular contrasts. In $T2_w$, the signal from the Fat-TMM (PVCP) was lower than the signal from the muscle, which does not correspond to the expected tissular contrasts (Fig. 3).

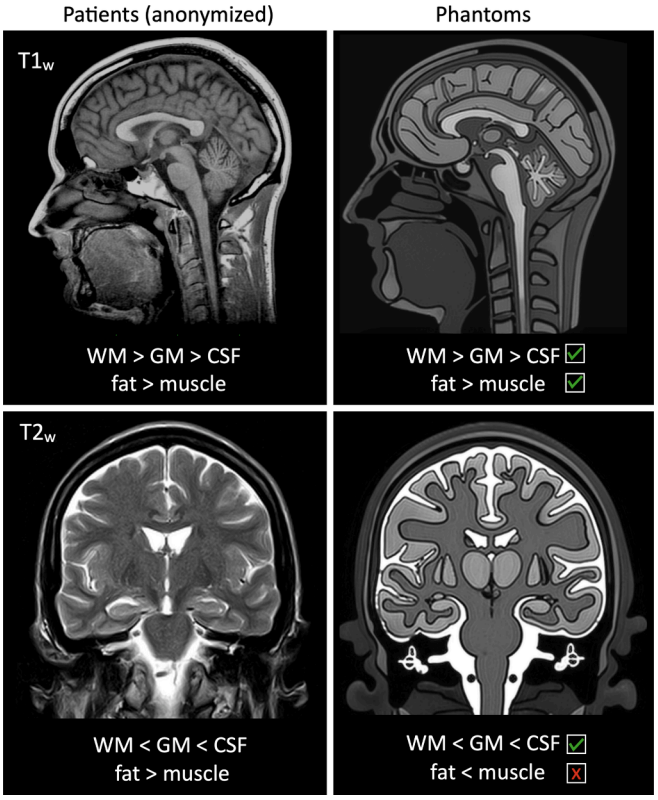

Fig. 3. Comparisons between real human acquisitions (left) and our phantoms (right) in fundamental MRI contrasts ($T1_w$, $T2_w$). Relative intensities comparisons between white matter (WM), gray matter (GM) and cerebrospinal fluid (CSF); and fat and muscle. In $T1_w$: TMMs (WM, GM, CSF, Fat, Muscle) relative intensities-ranking match with patient contrasts. In $T2_w$: TMMs relative intensities ranking match with patient contrasts for nervous tissues (WM, GM, CSF); but fat-TMM intensity is to low in our phantoms and doesn't correspond with reality due to the relaxations properties of the TMM we use (PVCP).

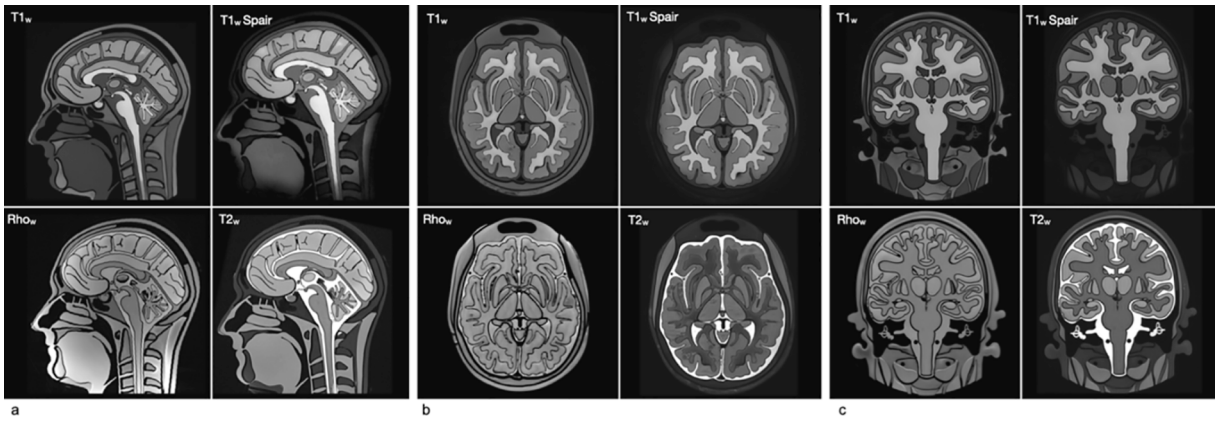

Fig. 2. MRI results of the sagittal (a), axial (b) and coronal (c) head phantom in different contrasts ($T1_w$,$T1_w$Spair, Rho_w and $T2_w$).

Fig. 4. Image quality comparison between acquisition 1 (a) and acquisition 4 (b) (see Table 3). We can see that truncation artefacts (black arrowhead) are more pronounced on acquisition 1 (a), while anatomical details are more visible (white arrowhead) on acquisition 4 (b). This is linked to the increase in the size of the acquisition matrix (see Table 3). The use of these phantoms therefore looks interesting both for qualitative analysis of sequences and for training in normal anatomy.

4. Discussion

4.1. High anatomical and contrast fidelity

Anatomically, these phantoms exhibit a high number of identifiable structures corresponding to key anatomical features routinely recognized in clinical practice (Figs. 2-4). Despite the presence of 0.4 mm PETG separation walls between different anatomical structures and tissues, they do not hinder anatomical analysis. The number of anatomical structures on our phantoms corresponds to clinical expectations; for example, we were able to position more than 40 anatomical structures on our coronal and transversal phantoms (Fig. 4a and 4b), and more than 80 structures on the sagittal section (Fig. 4c and 4d). To our knowledge, these phantoms provide the highest anatomical fidelity reported to date [6–11,19].

The gels used offer weighted contrasts matching clinical reality for white and gray matter, CSF, and muscles (Fig. 2). PVCP enables spectral fat suppression methods in T1-weighted images ($T1_w$ versus $T1_w$-SPAIR); however, T2-weighted images show low-intensity fat signals due to PVCP's relaxometric properties (short T2: 40–60 ms), mimicking fat suppression methods in T2-weighted sequences. At this stage, T2-FLAIR techniques are not accessible because the CSF TMM used does not have the same T1 relaxometry as the actual CSF. Additionally, the properties of the gels used do not allow for diffusion weighted imaging (DWI) contrast. Achieving this level of realism requires extensive gel design work, which we have not undertaken in this study. The development of precise gels remains a challenge that we have not yet overcome in this work. Also, in future works, contrasts between TMM will have to be evaluated quantitatively, using ROI to calculate contrast-to-noise ratios, for instance.

4.2. Technical points for improvement

We did not perform relaxometric acquisitions (T1 and T2 mapping). Obtaining TMM with exact T1 and T2 relaxation times matching those of tissues is challenging, and we cannot guarantee the relaxometric properties or long-term stability of the gels used . Our phantoms have not undergone long-term stability tests. Unsealed gels risk dehydration and contrast changes, and mold growth is possible if not prepared in sterile

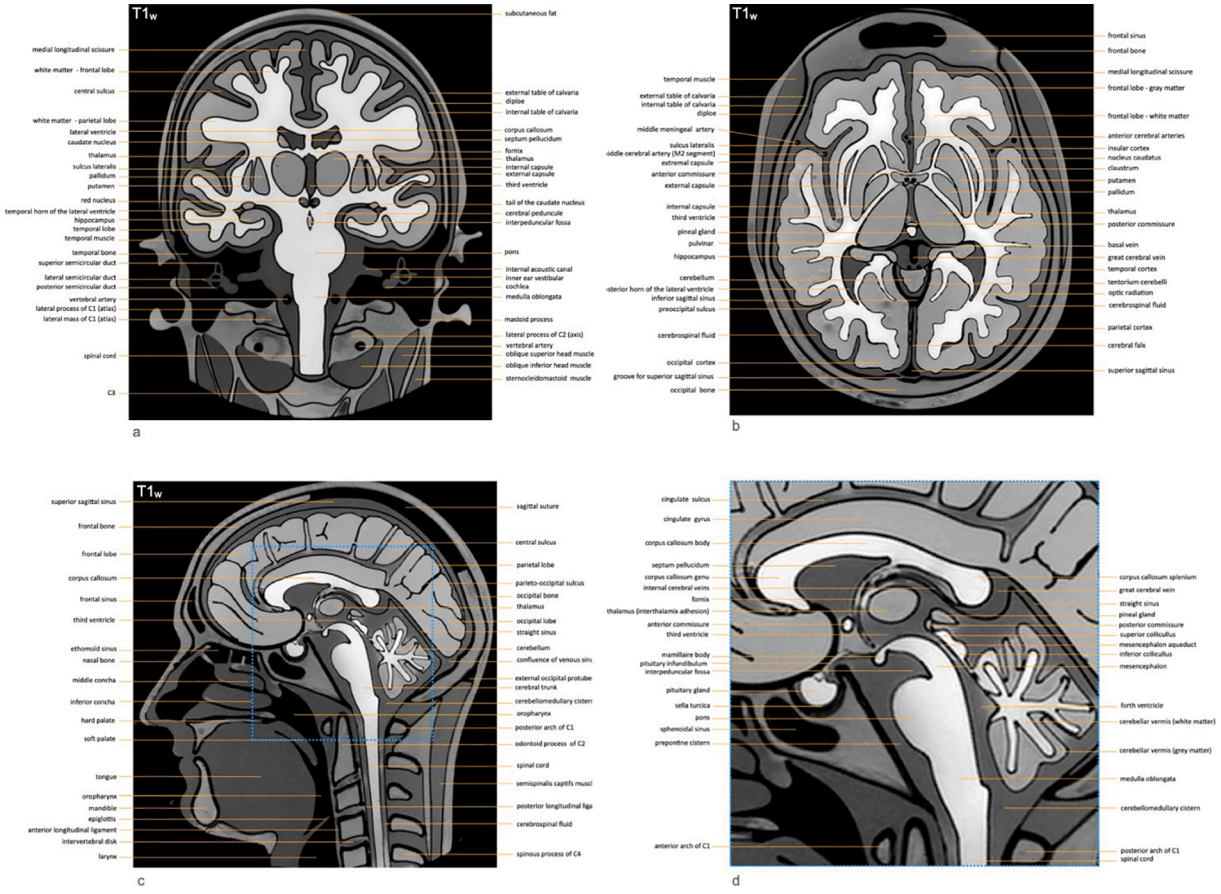

Fig. 5. Anatomical labelling of the sagittal head-phantoms in $T1_w$. Coronal slice phantom (a), transversal slice phantom (b), sagittal slice phantom (c) with magnification (d).

conditions or mixed with antibacterial chemicals or preservatives like NaN_3 [16]. In our experience, with NaN_3 preservative agents, the phantoms were store in a fridge at 4 °C for 2 months with no apparent problems. Air bubbles were observed in some areas, where dissolved gases adhered to the phantom walls as the gels cooled. In some cases, gelation occurs rapidly (in less than one minute), making it difficult to fill small structures. Filling these phantoms with Carrageenan-based agents (Table 2) was complex but relatively safe (no high temperatures). Regarding PVCP, its high temperature in the liquid state ($160 < T°C < 200°$) [18] risks melting the thin walls of PETG and its direct handling is dangerous (risk of burns). It is then necessary to wait (approximatively 5 min) that the temperature decreases without reaching a solid phase. These precautions make the filling of the phantoms complex.

4.3. Potential uses of these phantoms

Fig. 4 illustrates the potential use of these phantoms for optimizing MRI acquisition quality. However, this preliminary work is incomplete, precluding exhaustive conclusions on their usefulness for optimizing MRI sequences.

Pedagogically, these phantoms show promise for demonstrating the impact of parameter modifications on images; they have to potential to be precious tools to train students to recognize primary MRI contrasts ($T1_w$, $T2_w$, and Rho_w) and locate main anatomical elements.

Further works need to be undertaken to refine the formulation of the gels in order to achieve contrasts (and even relaxation times) as close as possible to human tissues. Also, an exhaustive assessment of these phantoms, including quantitative measurements (e.g. contrast-to-noise ratio, artefacts evaluations, etc) should also be conducted in the future. The democratization of 3D printing and the improvement of MRI gels (TMM) knowledge open possibilities for developing phantoms representing other anatomical regions (e.g., upper limbs, lower limbs, spine).

5. Conclusion

Our head phantoms demonstrate high anatomical and contrast fidelity but require technical improvements for stability and accurate T1 and T2 values over time. They offer a new way in education and sequence optimization and could be extended to other anatomical regions.

Grant support

This work of the Interdisciplinary Thematic Institute HealthTech, as part of the ITI 2021–2028 program of the University of Strasbourg, CNRS and Inserm, was supported by IdEx Unistra (ANR-10-IDEX-0002) and SFRI (STRAT'US project,ANR-20-SFRI-0012) under the framework of the French Investments for the Future Program."

Declaration of competing interest

The authors declare the following financial interests/personal relationships which may be considered as potential competing interests: Habeeb Yusuff reports financial support was provided by French National Research Agency. If there are other authors, they declare that they have no known competing financial interests or personal relationships that could have appeared to influence the work reported in this paper.

Data availability

The data (stl files) that support the findings of this study are available from the corresponding author upon reasonable request.

References

[1] Chen CC, Wan YL, Wai Y, et al. Quality assurance of clinical MRI scanners using ACR MRI phantom: preliminary results. J Digit Imaging 2004. https://doi.org/10.1007/s10278-004-1023-5.
[2] Panych LP, Chiou JYG, Qin L, Kimbrell VL, Bussolari L, Mulkern RV. On replacing the manual measurement of ACR phantom images performed by MRI technologists with an automated measurement approach. J Magn Reson Imaging 2016. https://doi.org/10.1002/jmri.25052.
[3] Wilcox PA, Hayden J, Lewis R, Froelich J. ACR MRI accreditation: yesterday, today, and tomorrow. J Am Coll Radiol 2005. https://doi.org/10.1016/j.jacr.2004.11.004.
[4] Manohar S, Sechopoulos I, Anastasio MA, Maier-Hein L, Gupta R. Super phantoms: advanced models for testing medical imaging technologies. Commun Eng 2024;3(1):73. https://doi.org/10.1038/s44172-024-00218-z.
[5] Phillips M. How volunteering for an MRI scan changed my life. Phys Rev E 2004;69:036109.
[6] Kilian D, Puderbach M, Bonekamp D, et al. 3D Extrusion printing of biphasic anthropomorphic brain phantoms mimicking mr relaxation times based on alginate-agarose-carrageenan blends. ACS Appl Mater Interfaces 2022. https://doi.org/10.1021/acsami.2c12872.
[7] Kraft M, Schick F, Schmidt R, et al. Towards a barrier-free anthropomorphic brain phantom for quantitative magnetic resonance imaging: Design, first construction attempt, and challenges. PLoS One 2023. https://doi.org/10.1371/journal.pone.0285432.
[8] Gopalan K, Johnson GA, Badea A. Quantitative anatomy mimicking slice phantoms. Magn Reson Med 2021. https://doi.org/10.1002/mrm.28740.
[9] Crasto N, Kirubarajan A, Sussman D. Anthropomorphic brain phantoms for use in MRI systems: a systematic review. Magn Reson Mater Phy 2022. https://doi.org/10.1007/s10334-021-00953-w.
[10] Kozana A, Eleftheriou A, Chalak L, et al (2018) Neonatal brain: fabrication of a tissue-mimicking phantom and optimization of clinical T1w and T2w MRI sequences at 1.5 T. Phys Med DOI: 10.1016/j.ejmp.2018.10.022.
[11] Rice JR, Hayes R, Tarbox L, et al. Anthropomorphic MRS head phantom. Med Phys DOI 1998;10(1118/1):598306.
[12] McGarry CK, Grattan LJ, Ivory AM, et al. Tissue mimicking materials for imaging and therapy phantoms: a review. Phys Med Biol 2020. https://doi.org/10.1088/1361-6560/abbd17.
[13] Antoniou A, Damianou C. MR relaxation properties of tissue-mimicking phantoms. Ultrasonics 2022. https://doi.org/10.1016/j.ultras.2021.106600.
[14] Antoniou A, Matzaroglou C, Bafitis I, et al. MR relaxation times of agar-based tissue-mimicking phantoms. J Appl Clin Med Phys 2022. https://doi.org/10.1002/acm2.13533.
[15] Woletz M, Schwarz M, Kainz W, et al. Human tissue-equivalent MRI phantom preparation for 3 and 7 Tesla. Med Phys 2021. https://doi.org/10.1002/mp.14986.
[16] Kato H, Matsuoka A, Yoshimoto M, et al. Composition of MRI phantom equivalent to human tissues. Med Phys 2005;10. https://doi.org/10.1118/1.4790023.
[17] Kim MJ, Choi HS, Han KJ, et al. Development of a hybrid magnetic resonance/computed tomography-compatible phantom for magnetic resonance guided radiotherapy. J Radiat Res 2020. https://doi.org/10.1093/jrr/rrz094.
[18] Chatelin S, et al. Investigation of PolyVinyl chloride plastisol tissue-mimicking phantoms for MR-and ultrasound-elastography. Front Phys 2020. https://doi.org/10.3389/fphy.2020.577358.
[19] Meerbothe TG, Florczak S, Van den Berg CAT, Levato R, Mandija S. A reusable 3D printed brain-like phantom for benchmarking electrical properties tomography reconstructions. Magn Reson Med 2024. https://doi.org/10.1002/mrm.30189.